# Addressing the environment electrostatic effect on electron transport in large systems: a QM/MM-NEGF approach

Gustavo T. Feliciano,*,† Carlos Sanz-Navarro,¶ Mauricio Domingues Coutinho-Neto,‡ Pablo Ordejón,¶ Ralph H. Scheicher,§ and Alexandre Reily Rocha*,‖

†*Instituto de Química, Departamento de Fisico-Química, Universidade Estadual Paulista (UNESP), Araraquara, SP, Brazil*

‡*Centro de Ciências Naturais e Humanas, Universidade Federal do ABC, Santo André, São Paulo, Brazil*

¶*Catalan Institute of Nanoscience and Nanotechnology (ICN2), CSIC and The Barcelona Institute of Science and Technology, Campus UAB, Bellaterra 08193 Barcelona, Spain*

§*Division of Materials Theory, Department of Physics and Astronomy, Uppsala University, Uppsala, Sweden*

‖*Instituto de Física Teorica, Universidade Estadual Paulista (UNESP), São Paulo, SP, Brazil*

E-mail: gtroiano@iq.unesp.br; reilya@ift.unesp.br
Phone: +55 (16) 3301 9869

## Abstract

The effects of the environment in nanoscopic materials can play a crucial role in device design. Particularly in biosensors, where the system is usually embedded in a solution, water and ions have to be taken into consideration in atomistic simulations of electronic transport for a realistic description of the system. In this work we present a methodology that combines quantum mechanics/molecular mechanics methods (QM/MM) with the non-equilibrium Green's function (NEGF) framework to simulate the electronic transport properties of nanoscopic devices in the presence of solvents. As a case in point we present further results for DNA translocation through a graphene nanopore. In particular we take a closer look into general assumptions in a previous work[1]. For this sake, we consider larger QM regions that include the first two solvation shells and investigate the effects of adding extra k-points to the NEGF calculations. The transverse conductance is then calculated in a prototype sequencing device in order to highlight the effects of the solvent.

## 1 Introduction

Manipulation of electronic properties of matter at the nanoscale could allow for the design of potentially revolutionary devices. In the particular case of biosensors - where a biological molecule interacts with an analyte for detection - the dimensions of the device are compatible with biological molecules, and one can envision sensing reaching the single-molecule level. A particular type of biosensor is a DNA sequencing device.[2,3] This is a process where the order of the nucleobases in a DNA molecule is determined, depending on the interaction of each

nucleotide with a given sensor device. Recently, nanopores have been heralded as the path towards single-molecule sequencing.[4–9] In such devices, the DNA molecule is driven through a pore, where each nucleobase can selectively interact with the device. Detection is then obtained by measuring the current, while a particular nucleotide is present in the pore, *i.e.* using a resistive biosensor. In principle, one can use either biological entities for detection, such as protein translocation channels or non-biological ones, such as silicon nitride or graphene nanopores.[3]

Typically, biological molecules are immersed in a solution containing a solvent - mostly water and salt, in different concentrations. Removal from this solution, in many cases, leads to significant changes in structure and function.[10] Thus, in the design of a biosensor, the dielectric effect of the environment might be crucial.[11] Fluctuations in the atomic configuration of the environment most likely change the potential seen by the device, which in turn could alter the behavior of the current-voltage curve in a resistive biosensor.

From the theoretical point of view, performing *ab initio* molecular dynamics (AIMD) of the full system whilst simulating the electronic transport is, up to the present point, still prohibitively expensive to be carried out. A possible workable strategy is to separate the structure generation step from the transport calculation step. Empirical molecular dynamics simulation (MD) is employed to sample over possible atomic configurations that represent the system, and then Density Functional Theory (DFT) is used[12,13] to obtain the electronic structure and the system Hamiltonian. Transport calculations are then performed within the non-equilibrium Green's Function (NEGF) method.[14]

Still, with a few exceptions[15], the solvent is only taken into account in the configurational sampling. Thus, the environment is usually not explicitly considered in the electronic structure / electron transport calculations, especially when the calculation involves biological systems.[16–18] In one of the first works to try to address the effect of a dielectric environment on electron transport by considering water explicitly in the electron transport calculation - up to 360 molecules[19] it was demonstrated that, when the molecular system attached to the electrodes is polar, the environment screens part of the electric dipole, causing shifts in the transmission spectrum. When the molecule is non-polar, the time-averaged electric field from the environment is close to zero, and the average shift in the transmission is much smaller.

Given that the number of atoms present in biosensor models is very large once the environment is explicitly taken into account, additional approximations must be employed. The hybrid QM/MM approach[20–22] divides the system Hamiltonian into a QM region, where atoms are treated quantum mechanically, and a MM region, where atoms are treated by classical force field methods. This partition allows for the treatment of very large systems. The interaction between the two sub-systems is included by using typical classical Coulomb and van der Waals terms so that the environment is represented by an external electrostatic potential for the QM part. The limitation of this approach is that one neglects charge transfer between the QM and MM parts and typically also the MM subsystem polarization.

In a recent work[1], a NEGF methodology allied to a QMMM description of the environment was used, in order to elucidate the effect of many water molecules, counterions and a few nucleobases on the zero-bias conductance of a graphene-based DNA sequencing device. The chosen system is one of the most promising systems for DNA sequencing and detection, and yet, due to its small thickness, it is also highly exposed to the environment. In this particular study, the chosen QM system was only the nucleotide and the nanopore. It was shown that the solvent modulates the charge transfer between the nucleobase and the nanopore, and the precise environment description is crucial to understand the working mechanism of the sensor.

In this work, we propose a deeper analysis in the NEGF-QMMM electron transport calculation protocol, illustrating its application on the same system, with a detailed analysis on

the effect of the environment on specific details of the electronic structure and electrostatic potential, and also including k-point sampling in the transport calculation, and also the effect of other alternative QM/MM partitions, including water molecules in the QM region, offering more insight in the QM/MM-NEGF application protocol.

# 2 Computational methods: The QM/MM-NEGF protocol

The prototypical device we are considering consists of two metallic terminals coupled via a so-called scattering region. In the particular case of a nanopore used for DNA sequencing, the electrodes consist of pristine graphene (a unit cell of the semi-infinite electrodes and the scattering region would, in principle, be a graphene sheet containing the nanopore, a strand of DNA that is sieved through the pore, water molecules and the counter-ions. A typical setup is shown in Figure 1A.

In order to obtain the electronic transport properties one can use a Green's function approach to obtain the low-bias conductance[14,23–25]

$$\sigma = \frac{2e^2}{h} T\left(E_F\right) \ , \tag{1}$$

where $G_0 = 2e^2/h$ is the quantum of conductance, and $T\left(E_F\right)$. is the total transmission at the Fermi level. In turn, the transmission can be obtained via Green's functions for the open system[26–29]

$$T\left(E\right) = \Gamma_L\left(E\right) G^{\dagger}\left(E\right) \Gamma_R\left(E\right) G\left(E\right) \ , \tag{2}$$

where $\Gamma_\alpha = i\left[\Sigma_\alpha - \Sigma_\alpha^{\dagger}\right]$ $(\alpha \equiv \{\mathrm{L}, R\})$, $\Sigma_{L/R}$ are the self-energies[14,30,31] - the effect of the semi-infinite electrodes on the scattering region - and

$$G^R\left(E\right) = \left[\epsilon^{+} S_S - H_S - \Sigma_L\left(E\right) - \Sigma_R\left(E\right)\right]^{-1} \ , \tag{3}$$

is the retarded Green's function for the scattering region, and $\epsilon^{+} = E + i\eta$. The key point is to obtain the QM Hamiltonian $H_S$ (and overlap matrix $S_S$) descring the scattering region. Ideally this would entail writing a single particle Hamiltonian in a localized basis set for all the atoms shown in Figure 1A.

Furthermore, given the dynamic nature of the problem, one would require sampling over a set of structural configurations. For this sake, a classical parameterization of the system's Hamiltonian is employed for the time evolution of the atomic coordinates. In this case, AMBER is a very well suited parametrization for biomolecular systems. The atomic configuration of the system is obtained from a classical molecular dynamics trajectory, which is a technique accurate enough to significantly sample the configurational space.

Given the atomic coordinates of the system, its electronic structure can be obtained. Further simplification of the problem is possible if we note that electron flow occurs in a limited region, in the case of a device in aqueous solution. The effect of most of the solvent is electrostatic in nature. The same problem is faced in a number of problems involving biomolecules. This is dealt with by using a hybrid quantum mechanics/molecular mechanics partition,[21] that is, an environment described by classical force field partial charges acting electrostatically over a subset of the system described by quantum mechanics, where electrons are explicitly taken into account.

This is especially valid, as long as electronic reorganization is restricted to the quantum region (QM). In this sense, the classical region (MM) creates a potential that only polarizes the quantum charge density, and no charge is transferred between the regions. It is a multi-scale approach that allows the treatment of thousands of atoms.[32,33]

The quantum-mechanical subsystem is usually treated by first-principles calculations based on density functional theory (DFT).[12,13], and the MM electrostatic potential is evaluated from the force field's partial charges. Once the QM and the MM systems are defined, the QM/MM electrostatic coupling Hamiltonian is

calculated

$$E_{QM/MM} = \sum_{i=1}^{C} q_i \int \frac{\rho(\vec{r})}{\vec{r} - \vec{r}_i} d\vec{r} + \sum_{i=1}^{C} \sum_{j=1}^{Q} \frac{q_i Z_j}{\vec{R}_j - \vec{r}_i} \quad (4)$$

where $q_i$ are the partial charges of the MM system, $\vec{r}_i$ is the vector position of the $i$-th partial charge, $\rho(\vec{r})$ is the electron density in the QM region and $Z_j$ is the nuclear charge of the $j$-th QM nuclei and $\vec{R}_j$ its respective vector position. In our case, the MM electrostatic potential was calculated using a QM/MM implementation in SIESTA,[34,35]. The MM potential is also fully periodic, with the same lattice vectors of the QM system. In the DFT framework, the calculated potential is directly added to the Hartree potential, until self-consistency is achieved in the electronic charge density of the QM region.

When the QM/MM boundary is defined across a covalent bond, a specific description for the frontier must be used. The most common solution is the scaled position link-atom method[36] (SPLAM), where the valence of the QM region is completed by adding hydrogen atoms along the frontier bond.

Finally, it is important to note that the electron transport calculation requires well defined boundary conditions between the scattering region and the electrodes. Since the external potential in this region can fluctuate due to the presence of the solvent, we smoothly truncated the MM potential to zero at this region, using a Fermi-Dirac-like smoothing function. This guarantees a smooth matching between the scattering region and the left and right electrodes.

In essence, we perform a three-step procedure, namely first a classical molecular dynamics simulation to obtain a set of configurations. They are subsequently used, by appropriately partitioning the system, in a single point QM/MM calculation. With the Kohn-Sham Hamiltonian we calculate the transmission probability as a function of energy.

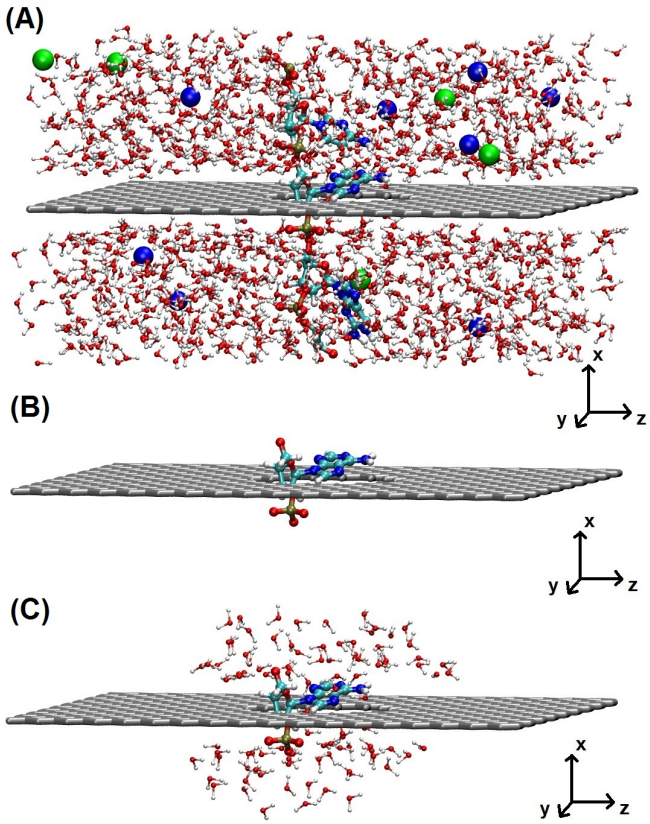


Figure 1: (A) Atomistic Illustration of the system, composed by graphene, DNA, water and counterions. (B) The QM partition A composed of graphene and a nucleotide (C) The QM partition B, same as the partition A, plus a layer of 8Å of surrounding water molecules

# 3 Results

The protocol was applied to the study of the electron transport across graphene sheet containing a nanopore through which a a DNA molecule is translocated. This is a prototype system for DNA electronic sequencing, where the effect of the chemical environment is potentially significant.

## 3.1 System construction and configurational sampling

The graphene nanopore is constructed from a square-shaped graphene sheet of dimensions 4 nm × 4 nm containing a nanopore, with a central hexagonal-shaped orifice, approximately 1.3 nm wide, with the edges in the zigzag config-

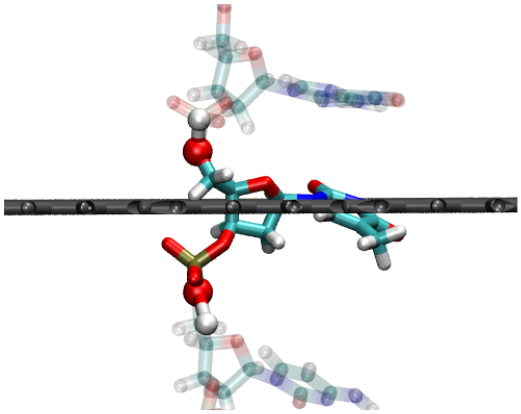

Figure 2: The frontier QM/MM covalent bonds defined for this work. The transparent part represents the DNA region described by the classical Hamiltonian. The link atoms are emphasized as spheres in the opaque region

uration. The size of the nanopore was chosen as a compromise between experimental fabrication feasibility[37,38] and consideration for the computational expenses of the simulations. The dangling bonds in the edge were saturated with hydrogen atoms. The graphene nanopore is composed of 615 atoms (see Figure 1).

A periodic single-stranded DNA molecule with 4 nucleotides (ATCG sequence) was inserted in the nanopore, and the system was completely immersed in water (4400 atoms) with 8 $Na^+$ and 4 $Cl^-$ counter ions at 0.1M concentration. The imbalance of 4 extra $Na^+$ ions compensates the 4 negative charges from the DNA phosphate groups. (Figure 1a).

As previously described, the configurational space is sampled by classical molecular dynamics (MD) simulations, employing the standard all-atom version of the AMBER99SB[39] empirical force field, implemented in the GROMACS[40] package, and the Particle-Mesh-Ewald (PME)[41] method is employed for the calculation of the electrostatic energy. We used the SPC water model[42] and parameters for benzene to model graphene, with partial charges only in the hydrogen atoms terminating the nanopore edges and their neighboring carbon atoms.

Four initial configurations are considered for DNA: in each, one of the four nucleotides is close to the pore. MD simulations are performed for each initial configuration, yielding 4 MD simulations. The system undergoes a thermalization procedure performed for 100 ps at 300 K using an $NVT$ ensemble. We then equilibrated the water density for a further 200 ps using an $NPT$ ensemble at 300 K and 1 bar with a Nose-Hoover thermostat[43,44] and Parrinello-Rahman barostat[45]. In both cases, each nucleotide is restricted inside the pore by a harmonic potential restriction, but allowing free movement within the plane of the graphene sheet. Finally, in the production stage, a 300 K $NVT$ 2000 ps MD simulation is performed in which all the atoms are free to move. The final frame of each MD simulation is taken as an input for the following calculations.

## 3.2 Electronic structure, QM/MM partition and NEGF calculations

For the next step, the electronic structure of the system is obtained for each frame from the MD simulations. Two different QM/MM partitions are considered in this work. Regarding the QM region composition, the partitions are: (A) graphene nanopore and one nucleotide (B) graphene nanopore, one nucleotide and a layer of water molecules within 8 Å of the nucleotide. In each partition, the MM region contains the rest of the system (water, counterions and remaining nucleotides).

The QM/MM covalent boundary is established across two chemical bonds in DNA, in the phosphate group connecting the QM nucleotide with its two neighbors. The link atoms are placed between the oxygen of one nucleotide and the carbon atom of the sugar ring linking to the next nucleotide. Thus, the QM system always has an overall -1e charge, and the MM environment has a +1e charge.

The quantum region (QM) is described using the generalized gradient approximation for the exchange and correlation potential in its PBE form[46]. Core electrons were replaced by norm-conserving pseudopotentials, fully factorized and using non-linear partial-core corrections for pseudo-wave-function smoothness

close to the nuclei. The Kohn-Sham wavefunctions for the valence electrons were expanded in a basis set of soft-confined, finite-support numerical atomic orbitals. A double-$\zeta$ polarized (DZP) basis set was used for the nucleotide atoms and a double-$\zeta$ (DZ) basis for the graphene membrane. The calculations were carried out with the SIESTA code[34], using a finite real-space grid corresponding to a 200 Ry plane-wave cutoff for the integrals in real space. The electrodes (L/R) are taken as pristine graphene sheets whereas the scattering region (S) consists of a piece of graphene containing the pore and one nucleobase.

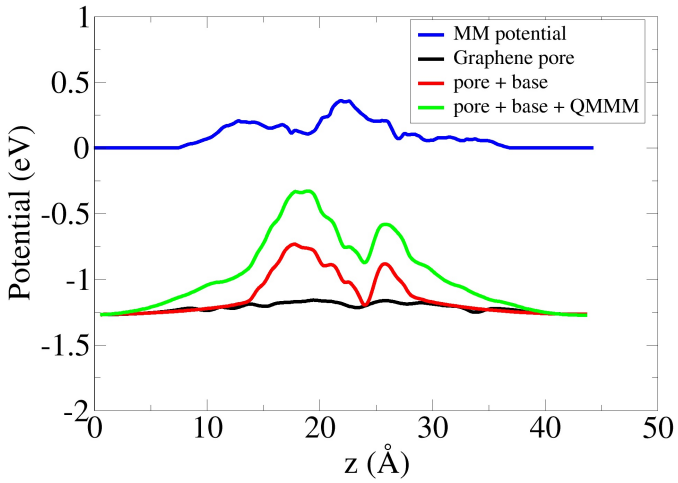


Figure 3: Macroscopically averaged electrostatic potential as a function of the z coordinate of one of the atomic configurations representing the graphene-nucleobase system, comparing the effect of each part of the system (bare pore, pore + nucleobase and pore + nucleobase + MM potential)

The classical region (MM) is described by the AMBER99SB force field parametrization. QM/MM interaction cutoff is 25.0 Å which is large enough to take all the remaining atoms in the MD frame into account in the classical region. The MM Coulomb potential is calculated by an Ewald summation.

Further analysis of the MM electrostatic potential, as shown in figures 3 and 4 reveals the extent of the environment action on the graphene/nucleobase system, along with the charge density difference. Figure 3 shows the macroscopically averaged electrostatic potential. Since the QM system is negatively charged, the MM potential is predominantly positive. As depicted by the colored surface maps, the electronic charge follows the external potential pattern, extending all over the graphene nanopore and the nucleobase. The potentials, however, are not additive, since the green curve comes from the electronic structure calculation under the MM potential, and therefore, the electronic structure is not the same as the calculation without the MM potential.

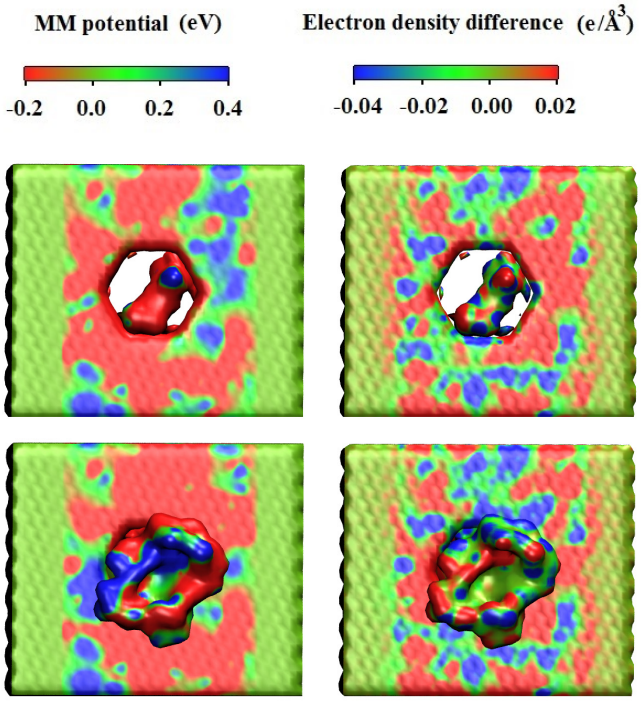


Figure 4: Surface map of the electrostatic potential generated by the MM classical charges in QM/MM partition A (top left) and B (bottom left). Charge density difference upon inclusion of the QM/MM potential (top right and bottom right). Both maps are projected on an electronic isodensity surface of $10^{-4}$ e/Å$^3$

Figure 5 depicts the electronic projected density of states of the QM system in the chosen snapshots, under the QM/MM partition A. Without the QM/MM inclusion, there are electronic states of the phosphate group, close to the Fermi level. Upon inclusion of the MM potential, these states change in energy, as the phosphate negative charge is stabilized on the oxygen atoms. Some states generated from hybridization of the orbitals on the nucleobase

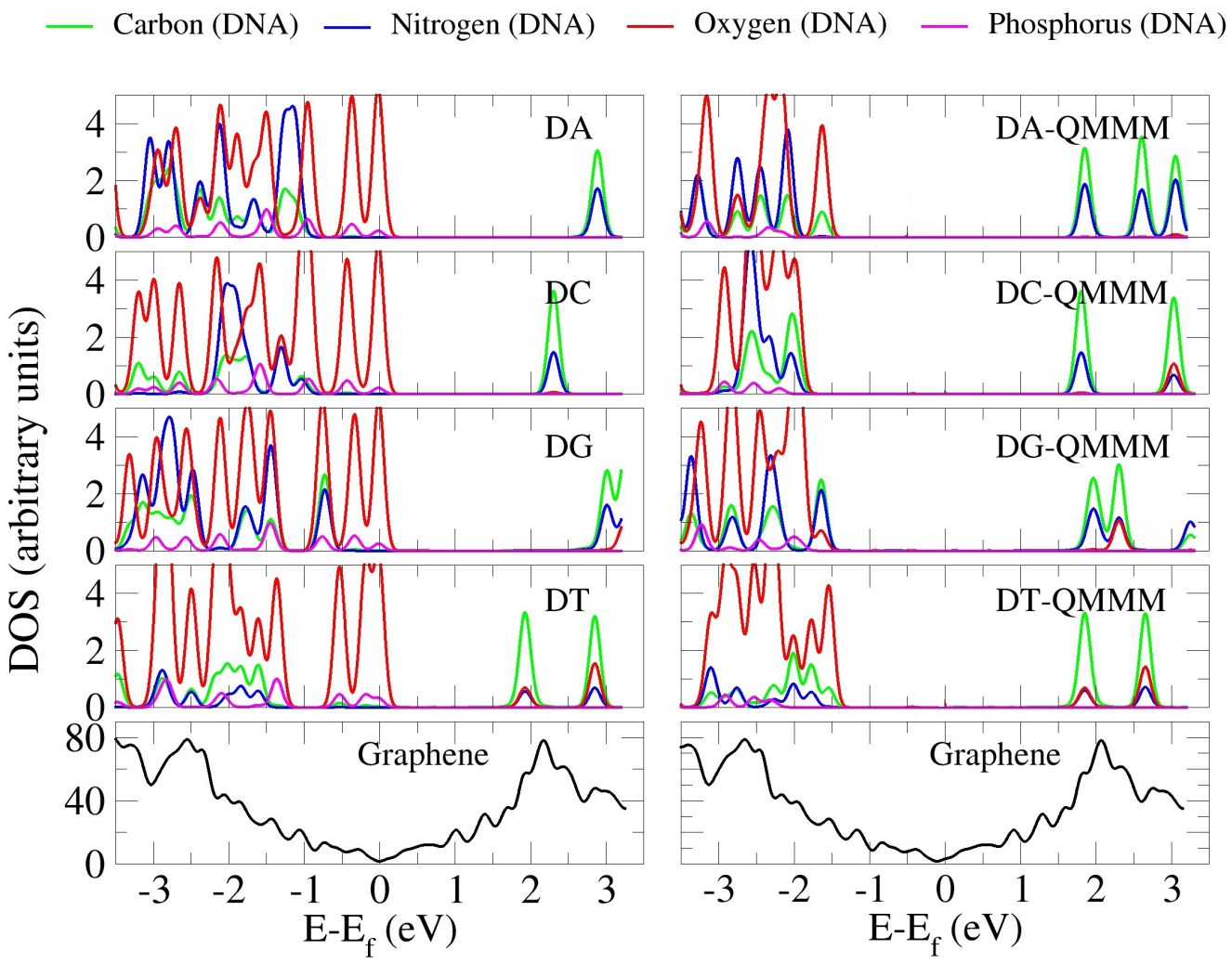


Figure 5: Projected DOS of the graphene-nucleobase systems, for the QM/MM partition A

region get closer to the Fermi level from positive values, which have a significant contribution from nitrogen and carbon atoms from the nucleobase ring moieties.

Figure 6 illustrates the projected density of states, but in the QM/MM partition B. Now the system has water molecules in the QM region, and display a remarkable contribution very close to the Fermi level, in the absence of the MM potential. In the presence of the MM potential, the water states also redistribute in energy. Comparing to the results of the partition A, the inclusion of water molecules in the QM region already change the behavior of the phosphate moiety, and the negative charge is stabilized upon it even without the MM potential. However, many other states from the QM water molecules appear close to the Fermi level, which can be associated to DFT's self interaction problem, already reported in similar studies[19]. Inclusion of the MM potential on partition B moves these states away from the Fermi level, and describe the same shift in the nucleobase electronic states as the QM/MM calculation on partition A.

Figure 7 shows the transmission spectrum difference between the calculation in each QM/MM partition, for each of the chosen snapshots (one for each nucleobase). At the Fermi level, there are differences of the order of 0.02, but the differences are significantly larger when looking at the spectrum at other energies.

In can be seen that the presence of the nucleotide, along with the MM potential leads to changes in the charge distribution around the pore, and consequently to changes in the

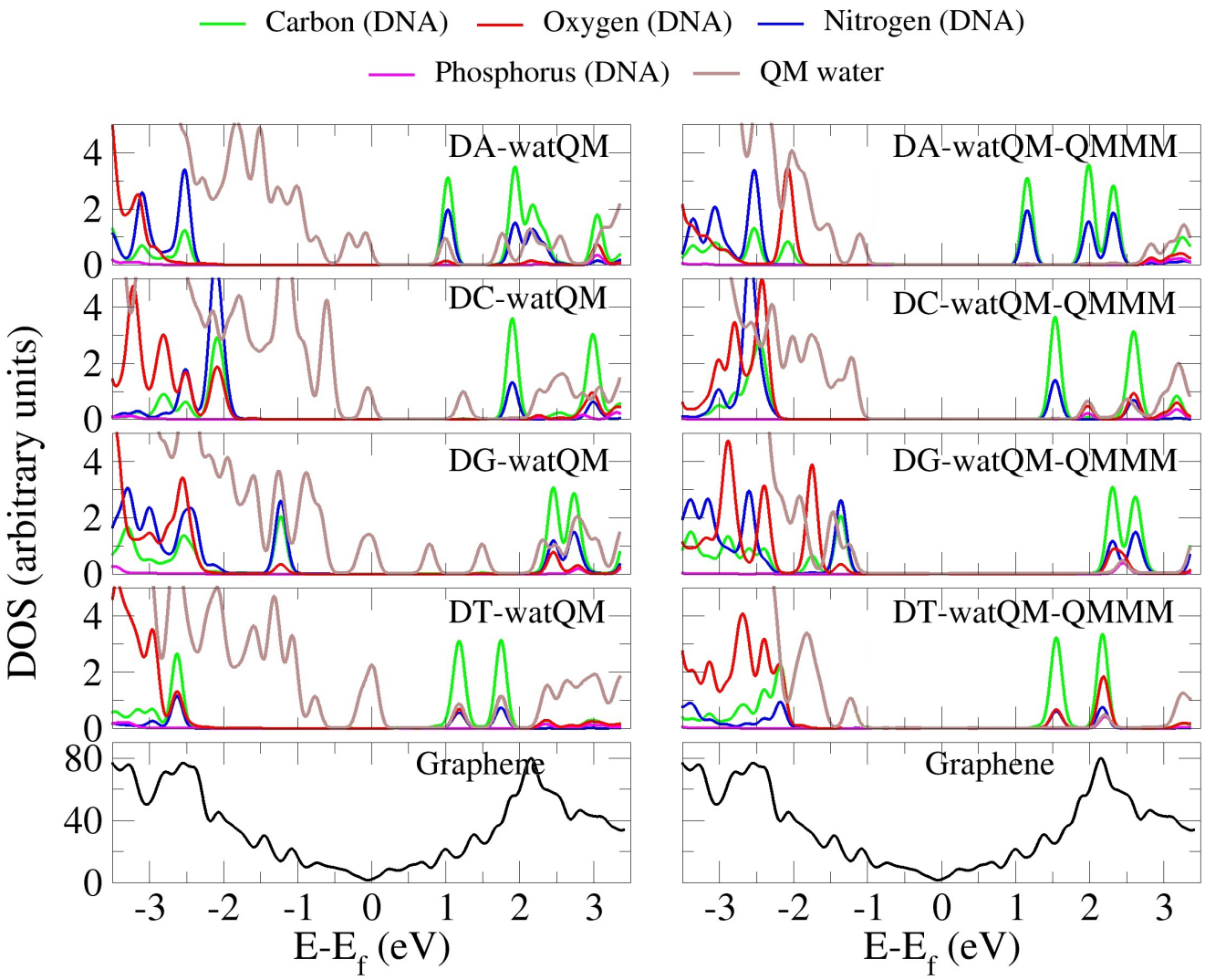


Figure 6: Projected DOS of the graphene-nucleobase systems, for the QM/MM partition B. The DOS from water molecules in the QM region are downscaled by a factor of 5

conductance, since the PDOS analysis shows negligible contribution of the nucleobase states at the electrode Fermi level in all studied QM/MM partitions. Zero-bias conductance changes come mainly from the shift of the graphene states lying close to the electrode Fermi level, in response to the changes in the electronic structure of the DNA and the graphene pore, which in turn come from the inclusion of the MM potential.

Therefore all the effects seen in the calculation suggest an electrostatic gating role for the environment. The change in the charge of the DNA and the atoms in the nanopore in turn alter the position of the electronic states involving graphene. Such feature is easily taken into account under the proposed methodology.

# 4 Conclusions

In this work, we employ the QM/MM-NEGF electron transport calculation protocol for a detailed decription of the effect of the environment over the transmission properties of a graphene-based DNA electronic sequencing device. There are significant changes that the model can capture upon the inclusion of the environment, and the method allows for the inclusion of large systems (composed by thousands of atoms) with low computational cost. Another interesting advantage is that the parametrized MM charges, based on high level quantum chemical calculations and potential fitting to classical charges, enforce the expected distribution of charge, avoiding DFT excessive charge

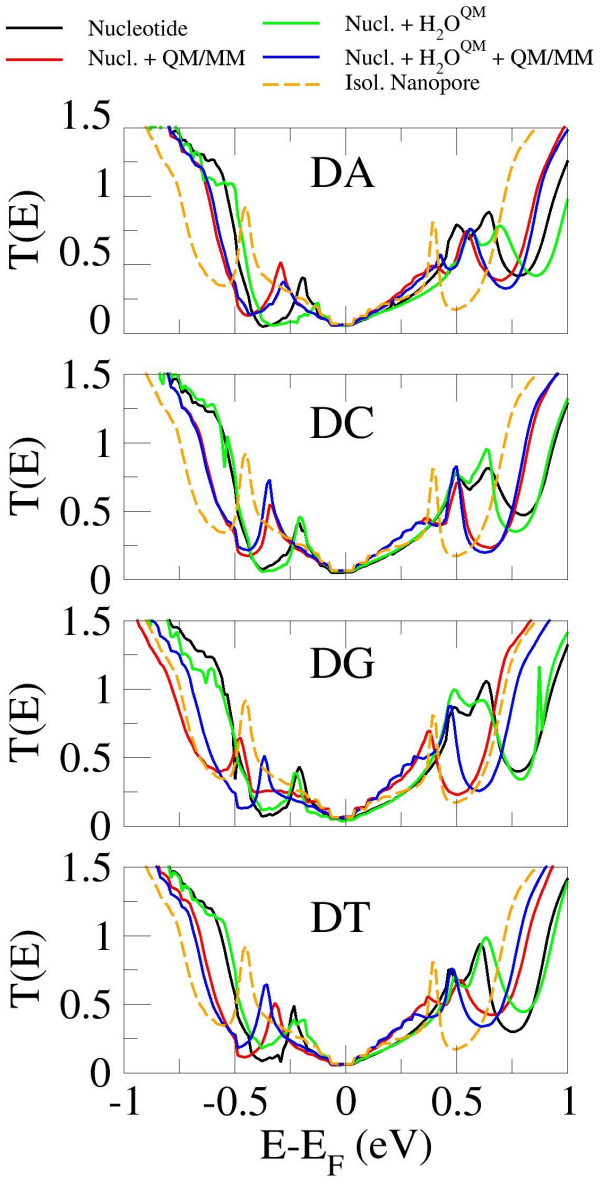


Figure 7: Zero-bias transmission for all studied nucleobases, with 10 k-points, in the configurations: pure graphene (black) and graphene+nucleobase system in 4 situations: bare system (red), system + MM potential (blue), system + quantum water layer (green), system with quantum water layer with MM potential (orange)

delocalization, where the MM potential, being non-polarizable, acts as a constraint for the QM electron density. We also showed that the technique can be adapted to study the explicit contribution of the solvent/environment orbitals to generate the transmission channels, just by extending the QM/MM partition. However, the extent of the QM region is, by definition, not unique, and should be systematically tested. Another possible interesting improvement over the current implementation is the use of a polarizable force field in the molecular dynamics simulation, for a description of the point charges or the MM region, when the environment is significantly polarizable. All improvements can be incorporated in the current methodology to provide a reasonable description of the electrostatic effect of the environment on electron transport properties, as proposed in the QM/MM-NEGF protocol.

## 5 Acknowledgments

The authors thank FAPESP and UFABC for financial support. A. R. R. acknowledges support from ICTP-SAIRF (FAPESP project 2011/11973-4) and the ICTP-Simons Foundation Associate Scheme. Computer time was provided by IFT/Unesp and USP/Sampa institutions. R.H.S. thanks the Swedish Research Council for financial support. PO acknowledges support from the Spanish MINECO (Grant FIS2015-64886-C5-3-P and the Severo Ochoa Centers of Excellence Program Grant SEV-2013-0295), Generalitat de Catalunya Government (2014SGR301), and EU H2020-EINFRA-5-2015 MaX Center of Excellence (Grant 676598). C.S.N. acknowledges support from MINECO through the Ramon y Cajal Program.

## References

(1) Feliciano, G. T.; Sanz-Navarro, C.; Coutinho-Neto, M. D.; Ordejón, P.; Scheicher, R. H.; Rocha, A. R. Phys. Rev. Applied **2015**, 3, 034003.

(2) Vercoutere, W.; Akeson, M. Current Opinion in Chemical Biology **2002**, 6, 816 – 822.

(3) Heerema, S. J.; Dekker, C. Nature Nanotechnology **2016**, 11, 127–136.

(4) Clarke, J.; Hai-Chen,; Jayasinghe, L.;

Patel, A.; Reid, S.; Bayley, H. Nature Nanotechnology **2009**, 4, 265–270.

(5) Postma, H. W. C. Nano Letters **2010**, 10, 420–425, PMID: 20044842.

(6) Feng, J.; Liu, K.; Bulushev, R. D.; Khlybov, S.; Dumcenco, D.; Kis, A.; Radenovic, A. Nature Nanotechnology **2015**, 10, 1070–1076.

(7) Niedzwiecki, D. J.; Lanci, C. J.; Shemer, G.; Cheng, P. S.; Saven, J. G.; Drndic, M. ACS Nano **2015**, 9, 8907–8915.

(8) Di Ventra, M.; Taniguchi, M. Nature Nanotechnology **2016**, 11, 117–126.

(9) Deamer, D.; Akeson, M.; Branton, D. Nat Biotech 34, 518–524.

(10) P. W. Fenimore, B. H. M. F. G. P., H. Frauenfelder Proceedings of the National Academy of Sciences of the United States of America **2002**, 99, 16047–16051.

(11) Aryal, B. P.; ; Benson*, D. E. Journal of the American Chemical Society **2006**, 128, 15986–15987, PMID: 17165722.

(12) Hohenberg, P.; Kohn, W. Physical Review **1964**, 155.

(13) Kohn, W.; Sham, L. J. Phys. Rev. **1965**, 140, A1133.

(14) Datta, S. Electronic Transport in Mesoscopic Systems, 1st ed.; Cambridge University Press: Cambridge, 1995; pp 57–88.

(15) Krems, M.; Zwolak, M.; Pershin, Y. V.; Di Ventra, M. Biophysical journal **2009**, 97, 1990–1996.

(16) Lagerqvist, J.; Zwolak, M.; Di Ventra, M. Nano letters **2006**, 6, 779–82.

(17) McFarland, H. L.; Ahmed, T.; Zhu, J.-X.; Balatsky, A. V.; Haraldsen, J. T. The Journal of Physical Chemistry Letters **2015**, 6, 2616–2621, PMID: 26266743.

(18) Prasongkit, J.; Feliciano, G.; Rocha, A. R.; He, Y.; Osotchan, T.; Ahuja, R.; Scheicher, R. H. Scientific Reports **2015**, 5, 17560.

(19) Rungger, I.; Chen, X.; Schwingenschlögl, U.; Sanvito, S. Phys. Rev. B **2010**, 81, 235407.

(20) Sanz-Navarro, C. F.; Grima, R.; García, A.; Bea, E. a.; Soba, A.; Cela, J. M.; Ordejón, P. Theoretical Chemistry Accounts **2010**, 128, 825–833.

(21) Warshel, A.; Levitt, M. Journal of Molecular Biology **1976**, 103, 227–249.

(22) Sabin, J. R.; Brandas, E. Advances in Quantum Chemistry **2010**, 59, 1–416.

(23) Haug, H.; Jauho, A. P. Quantum Kinetics in Transport and Optics of Semiconductors; Springer Series in Solid-State Sciences; Springer Verlag, 1999.

(24) Rocha, A. Theoretical and Computational Aspects of Electronic Transport at the Nanoscale; Trinity College, 2007.

(25) Brandbyge, M.; Mozos, J.-L.; Ordejón, P.; Taylor, J.; Stokbro, K. Phys. Rev. B **2002**, 65, 165401.

(26) Landauer, R. IBM J. Res. Develop. **1957**, 1, 233.

(27) Büttiker, M.; Imry, Y.; Landauer, R.; Pinhas, S. Phys. Rev. B **1985**, 31, 6207.

(28) Landauer, R. Phys. Scr. **1992**, 110, 1402.

(29) Caroli, C.; Combescot, R.; Nozieres, P.; Saint-James, D. Journal of Physics C: Solid State Physics **1971**, 4, 916.

(30) Rocha, A. R.; Garcia-Suarez, V. M.; Bailey, S. W.; Lambert, C. J.; Ferrer, J.; Sanvito, S. Nature Materials **2005**, 4, 335–339.

(31) Rocha, A. R.; García-Suárez, V.; Bailey, S.; Lambert, C.; Ferrer, J.; Sanvito, S. Physical Review B **2006**, 73.

(32) Senn, H. M.; Thiel, W. Angewandte Chemie International Edition **2009**, 48, 1198–1229.

(33) Brunk, E.; Rothlisberger, U. Chemical Reviews **2015**, 115, 6217–6263, PMID: 25880693.

(34) Soler, J. M.; Artacho, E.; Gale, J. D.; García, A.; Junquera, J.; Ordejón, P.; Sánchez-Portal, D. J. Phys. Cond. Mat. **2002**, 14, 2745.

(35) Sanz-Navarro, C. F.; Grima, R.; García, A.; Bea, E. A.; Soba, A.; Cela, J. M.; Ordejón, P. Theoretical Chemistry Accounts **2010**, 128, 825–833.

(36) Crespo, A.; Scherlis, D. A.; Marti, M. A.; Ordejon, P.; Roitberg, A. E.; Estrin, D. A. Journal Of Physical Chemistry B **2003**, 107, 13728–13736.

(37) Merchant, C. a.; Healy, K.; Wanunu, M.; Ray, V.; Peterman, N.; Bartel, J.; Fischbein, M. D.; Venta, K.; Luo, Z.; Johnson, a. T. C.; Drndić, M. Nano letters **2010**, 10, 2915–21.

(38) Schneider, G. F.; Kowalczyk, S. W.; Calado, V. E.; Pandraud, G.; Zandbergen, H. W.; Vandersypen, L. M. K.; Dekker, C. Nano letters **2010**, 10, 3163–7.

(39) Hornak, V.; Abel, R.; Okur, A.; Strockbine, B.; Roitberg, A.; Simmerling, C. Proteins: Structure, Function, and Bioinformatics **2006**, 65, 712–725.

(40) Berendsen, H.; van der Spoel, D.; van Drunen, R. Computer Physics Communications **1995**, 91, 43–56.

(41) Darden, T.; York, D.; Pedersen, L. Journal of Chemical Physics **1993**, 98, 10089–10092.

(42) Berendsen, H.; Postma, J.; Gunsteren, W.; Hermans, J. In Intermolecular Forces; Pullman, B., Ed.; The Jerusalem Symposia on Quantum Chemistry and Biochemistry; Springer Netherlands, 1981; Vol. 14; pp 331–342.

(43) Hoover, W. G. Phys. Rev. A **1985**, 31, 1695–1697.

(44) Nose, S. The Journal of Chemical Physics **1984**, 81.

(45) Parrinello, M.; Rahman, A. Journal of Applied Physics **1981**, 52.

(46) Perdew, J. P.; Burke, K.; Ernzerhof, M. Phys. Rev. Lett. **1996**, 77, 3865–3868.